Nanostructural Organization in a Biredox Ionic Liquid

Roxanne Berthin, Alessandra Serva, Olivier Fontaine, Mathieu Salanne

Nanostructural Organization in a Biredox Ionic Liquid

Roxanne Berthin,[†,‡] Alessandra Serva,[†,‡] Olivier Fontaine,[¶,§] and Mathieu Salanne[*,†,‡,§]

†*Sorbonne Université, CNRS, Physico-chimie des Électrolytes et Nanosystèmes Interfaciaux, PHENIX, F-75005 Paris*

‡*Réseau sur le Stockage Electrochimique de l'Energie (RS2E), FR CNRS 3459, 80039 Amiens Cedex, France*

¶*School of Energy Science and Engineering, Vidyasirimedhi Institute of Science and Technology (VISTEC), Rayong, 21210, Thailand*

§*Institut Universitaire de France (IUF), 75231 Paris, France*

E-mail: mathieu.salanne@sorbonne-universite.fr

Abstract

Ionic liquids generally display peculiar structural features that impact their physical properties, such as the formation of polar and apolar domains. Recently, ionic liquids functionalized with anthraquinone and TEMPO redox groups were shown to increase the energy storage performance of supercapacitors, but their structure was not characterized so far. In this work we use polarizable molecular dynamics to study the nanostructuration of such biredox ionic liquids. We show that TEMPO nitroxyl functions tend to aggregate, while the anthraquinone groups favor stacked arrangements. The latter eventually percolate through the whole liquid, which sheds some light on the mechanisms at play within biredox ionic liquids-based supercapacitors.

TOC graphic

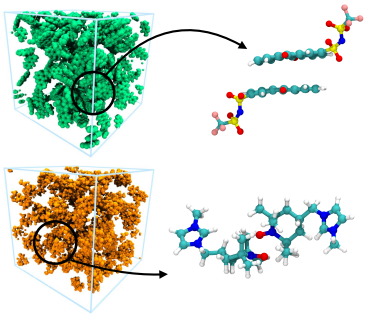

Over the past decades, the improvement of the energy storage performance of supercapacitors was mostly due to the discovery and the development of nanostructured electrode materials.[1] In principle, since the charging simply occurs through the adsorption of ions on the electrode counterbalanced by the accumulation of opposite charges on the surface, any conductive materials with large surface area could be used. This opened many possibilities for performance improvement, and systems based on nanoporous carbons,[2] 2D materials,[3,4] metal-organic frameworks,[5] etc. were extensively tested. The current commercial devices employ disordered nanoporous carbon electrodes, which allow for an efficient sieving of the ions, a fast diffusion of the electrolyte, and an excellent cyclability. Due to the presence of nanoconfinement effects, the conventional electrochemical double-layer picture was not able to describe accurately the systems, and it was necessary to develop adequate molecular simulations and spectroscopy techniques to fully understand the charging mechanisms of these supercapacitors.[6]

On the other side of the double-layer sits the electrolyte, which is generally a liquid. Here again, several families coexist: depending on the nature of the solvent and of the ions, different electrochemical windows and resistivities are obtained. Then for a given electrode material the capacitance may differ greatly between two electrolytes, so that its choice is generally driven by a compromise between these properties (and the cost).[7] The rise of ionic liquids (ILs) in the electrochemistry field brought many promises for supercapacitor applications.[8,9] Since they do not contain solvent, ILs were expected to yield larger capacitances than aqueous or organic solvent-based electrolytes. However, due to the large electrostatic attraction between cations and anions, they are less easily separated upon application of a voltage, and the capacitances remain comparable to the ones of organic solvent-based electrolytes.[10] It is only recently that several groups were able to take profit from the compositional flexibility and the unique structural properties of ILs to develop new capacitive mechanisms, in which the liquid plays an active role.[11–13] Mao *et al.* have developed surface-active ILs characterized by an amphiphilic structure inducing self-assembly at the electrode

interface. This lead to increased capacitance due to an enhanced separability of the ions.[11] In another work, biredox ILs (BILs) were synthesized by grafting both the cation and the anion with redox-active moieties that could exchange electrons with the electrode upon application of the voltage, leading to a two-fold to three-fold increase of the capacitance depending on the experimental conditions.[12] The most recent example is the use of hygroscopic protic ILs, in which water molecules are dispersed, that display higher energy and power performances than conventional ILs when used in supercapacitor devices.[13]

Although the use of redox-active electrolytes was far from being a new idea, in particular in aqueous electrolytes,[14–17] using BILs lead to particularly good performances, with a capacitance almost as large as the one of pseudo-capacitors but without sacrificing the fast charging ability of supercapacitors and their long-term cyclability, or leading to significant self-discharge effects as was usually the case in such systems. The reason behind this is not well understood, and it could stem from either the much larger concentration of ions inside the liquid or the nanostructuring effects which are very important in ILs.[18,19] However, so far the BIL-based supercapacitors were only studied by conventional electrochemical techniques that lack insight at the molecular scale. Since all the molecules bear redox moieties, it is very likely that the latter will interact closely within the liquid. Understanding these interactions is necessary for designing further BILs with enhanced properties.

Molecular dynamics simulation can provide significant information on the structure of electrolytes for supercapacitor applications.[20] Yet, compared to previous studies in which the atomic details of the ionic species were not important for catching the charging mechanisms,[21,22] in the case of BILs they certainly play a key role. Recently, we developed polarizable force fields for the 2,2,6,6-tetramethylpiperidinyl-1-oxyl (TEMPO) and anthraquinone (AQ) groups,[23] which opens the way for the simulation of BILs. In this work, we have simulated a BIL in which the imidazolium cation is functionalized with TEMPO ($TEMPOmIM^+$), while the bis(trifluoromethane)sulfonimide anion ($TFSI^-$) bears an AQ function ($AQTFSI^-$) as shown on Figure 1a and b. As in previous experimental work,[12,24] the simulation was per-

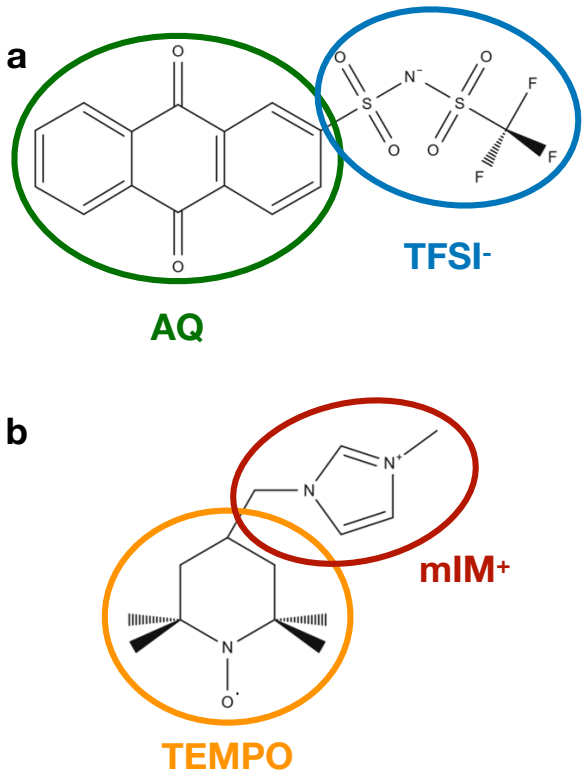

Figure 1: Structural formula of the studied biredox ionic liquid with the anion AQTFSI$^-$ (a) and the cation TEMPOmIM$^+$ (b). The various ionic and redox moieties are highlighted in green (AQ), blue (TFSI$^-$), orange (TEMPO) and red (mIM$^+$). This coloring scheme will be kept in the following.

formed at high temperatures because BILs display larger viscosity than generic ILs; here a value of 373 K was chosen.

In a generic IL, the intermolecular structure is dominated by Coulomb ordering effects. Due to the electrostatic interactions, the first shell of cations is mainly composed of anions and vice-versa. This ordering extends up to several solvation shells, leading to some ordering over the nanometer lengthscale.[25] The delocalization of the charge within the ions leads to additional structural features, such as the formation of apolar domains consisting of the alkyl chains of the molecules.[19] This effect can be exploited by using ILs as templating agents in chemical synthesis.[26] In the case of supercapacitors, it was exacerbated by synthesizing amphiphilic ILs in order to form self-assemblies at the electrode interface, leading to surface-active ILs.[11] Here the BILs differ from generic systems by including additional

redox functions, it is therefore of interest to analyze whether the latter modify the structural features of the liquid.

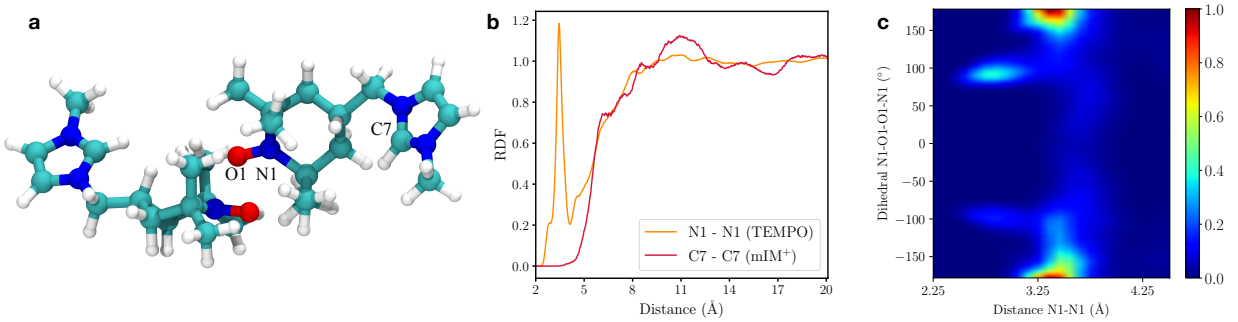

Figure 2: a) Typical snapshot showing the formation of a TEMPO-TEMPO dimer in the bulk BIL. b) Radial distribution functions (RDFs) between the N atoms (labelled N1 on panel a) from the TEMPO moieties (orange) and between the upper C atoms of the imidazolium ring (labelled C7 on panel a) of the mIM^+ moieties (red). c) Combined distribution function of the N1-O1-O1-N1 pseudo-dihedral angle (where O1 are the O atoms of TEMPO moieties as labelled on panel a) and the N1-N1 distance. The colormap reflects the occurrence probability.

Indeed, in the BIL, one can observe some new interactions arising from the affinity between the redox moieties. Firstly, the TEMPO groups tend to form dimers as illustrated on Figure 2a. The importance of the effect can be quantified from the comparison of the corresponding N1 - N1 radial distribution function (RDF) to the one of carbon atoms belonging to the cationic moiety of the molecule (C7 - C7). As shown on Figure 2b, the former exhibits a sharp peak at a short distance of 3.3 Å, while the latter is typical of ILs, with a very broad first "peak". The structural feature observed on Figure 2a is quite uncommon in ILs, and points towards a strong dipole-dipole interaction between the nitroxyl functions of the TEMPO. In order to check this observation, we computed the combined distribution function of N1-O1-O1-N1 dihedrals and N1-N1 distances, the results are plotted as density map on Figure 2c. At distances corresponding to the peak of the RDF, there is a clear preferential value of ± 180° for the pseudo-dihedral, which confirms this interpretation. We also note the existence of configurations with more closed angles (of approximately ± 100°) at shorter N1-N1 distances (which is characterized by a small shoulder on the corresponding

RDF). These arise from a situation where the N1 atom from the second molecule aligns with the N1-O1 bond of the first one, but the probability to find such configurations is much lower.

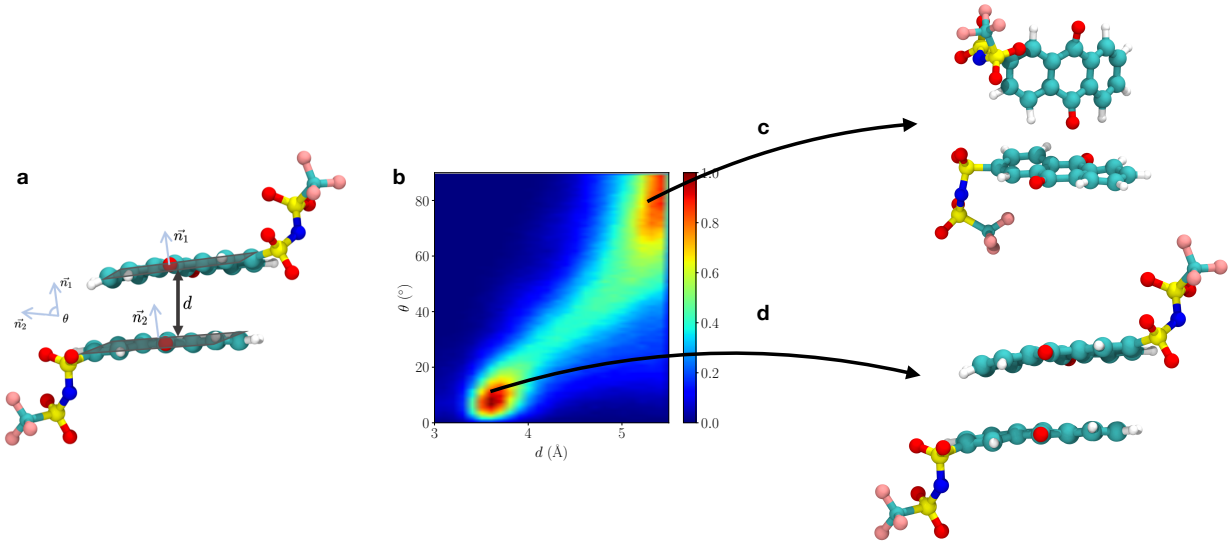

Figure 3: a) Typical snapshot of two stacked AQ moieties. The angle θ, i.e. the angle between the two normal vectors $\vec{n}_1$ and $\vec{n}_2$ to the two AQ pseudo-planes, and the distance d between them, which are used to characterize the degree of stacking, are also illustrated. b) Combined distribution function of θ and d. The colormap reflects the occurrence probability. c) Snapshot illustrating the *T-Shaped* stacking type. d) Snapshot illustrating the *Sandwich* stacking type.

Concerning the anions, structural organization of the AQ moieties were much more expected. Indeed, the anthraquinone has a well-known tendency to form stacked structures, an effect which has already proven important for energy storage applications.[27,28] Here we quantify the stacking as follow: first we define a distance d between each AQ quasi-planar moieties. To compute d, we determine for each AQ the position of the centers of mass of each ring (there are 3 of them per moiety). We then compute all the distances between each center of mass pair by pair (9 distances in each case) and d is taken as the smallest one. Then, we calculate the angle (θ) between AQ planes using the normal vector as illustrated on Figure 3a. This procedure allows us to construct a stacking map that shows the occurrence of each (d, θ) couple. It is shown on Figure 3b, where the color scale corresponds to the oc-

currence probability. We observe that two areas are highly likely: one at short distances and small angles that corresponds to the *Sandwich* stacking type (illustrated in Figure 3d) and a second one at large distances and wide angles that corresponds to the *T-Shaped* stacking type (illustrated in Figure 3c).

Generally, the presence of stacking is attributed to the existence of $\pi - \pi$ interactions between the AQ carbon rings. However, such interactions are not explicitly present in our model. Although they may arise effectively since the atomic charges and polarizabilities distributions were fitted from electronic structure calculations,[23] it is more likely that the stacking can be triggered by geometry effects and packing requirements only. We note that this effect can explain the solubility of BILs in acetonitrile, which is very low compared to the one of the parent IL mIM-TFSI that can be mixed at any concentration in this solvent.

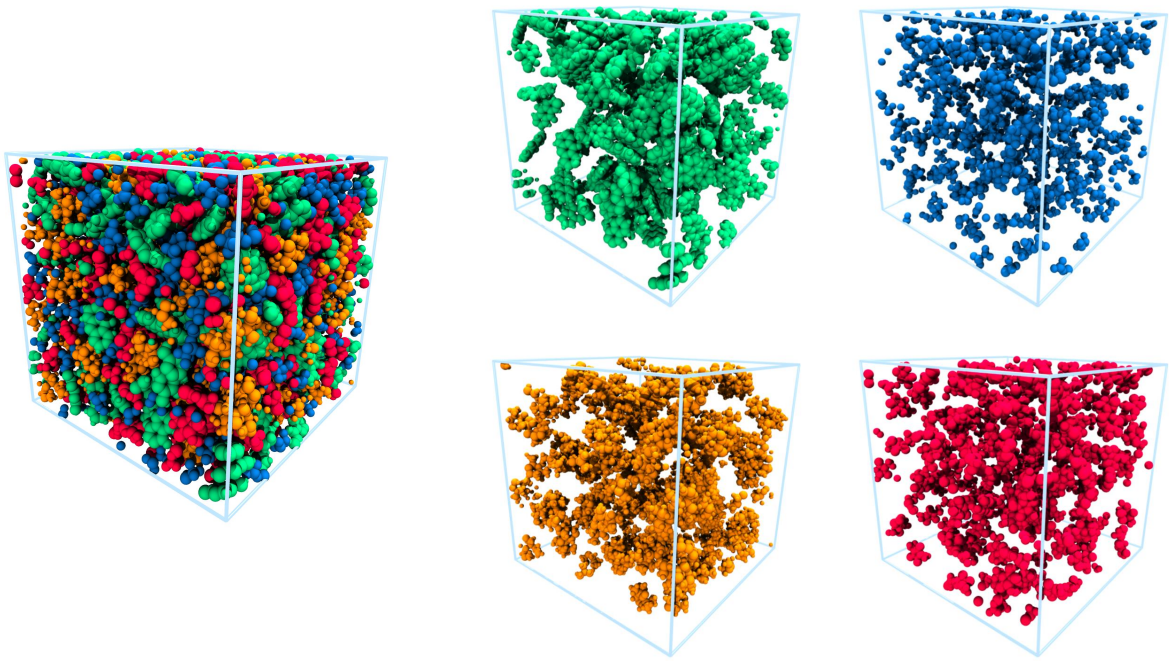

Figure 4: Snapshot of the BIL with distinct colors for each group of atoms. The ionic and redox moieties are in green for AQ, blue for $TFSI^-$, orange for TEMPO and red for mIM^+.

A strong affinity between TEMPO groups on the one hand and AQ groups on the other hand is thus observed in the BIL. On the contrary there is no particular structural organization occurring between TEMPO and AQ. This may lead to changes of the medium-range

Table 1: Domain analysis for the BIL moieties: average number of domains, surface and volume over the simulation.

	Average number of domains	Average surface (Å^2)	Average volume (Å^3)
TEMPO	6.18	5470	7452
mIM$^+$	7.78	4619	4210
AQ	2.04	24279	25624
TFSI$^-$	3.35	14065	14789

structure of the liquid compared to the one of the parent IL, the latter being mainly characterized by the formation of polar domains made of the ionic moieties of the mIM$^+$ and the TFSI$^-$ anions on the one hand, and of apolar domains made of the alkyl groups of the imidazolium (depending on the chain length) on the other hand. In ILs, it is generally useful to visualize the formation of such domains using specific coloring scheme, following the seminal work of Canongia Lopes and Padua.[18] On Figure 4 we show the overall BIL and the substructure formed by the TEMPO, AQ, mIM$^+$ and TFSI$^-$ groups. The formation of nanostructures is clearly evidenced, the effect looking more pronounced in the case of the TEMPO moieties.

In order to check this observation, it is possible to perform a quantitative domain analysis in the liquid using the TRAVIS software.[29,30] In short, the liquid is divided into each of the four defined building blocks. Then a Voronoi tessellation is performed, in which the polyhedra are constructed around the atomic sites. The building blocks are considered to form a domain if they share a common polyhedron face. Such an analysis was performed previously to investigate *e.g.* the templating effect of ionic liquids in which alcohol species are dissolved.[26] The results are summarized in Table 1, which provides for each type of group the average number of domains in the simulation cell, as well as their geometric features (average surface and volume). They confirm the visual observation since the AQ groups are splitted in two domains only on average, thus forming an almost continuous percolating structure. The clustering of the other groups is less pronounced, but we note again that even in the cations the TEMPO moieties form larger domains on average than the mIM$^+$.

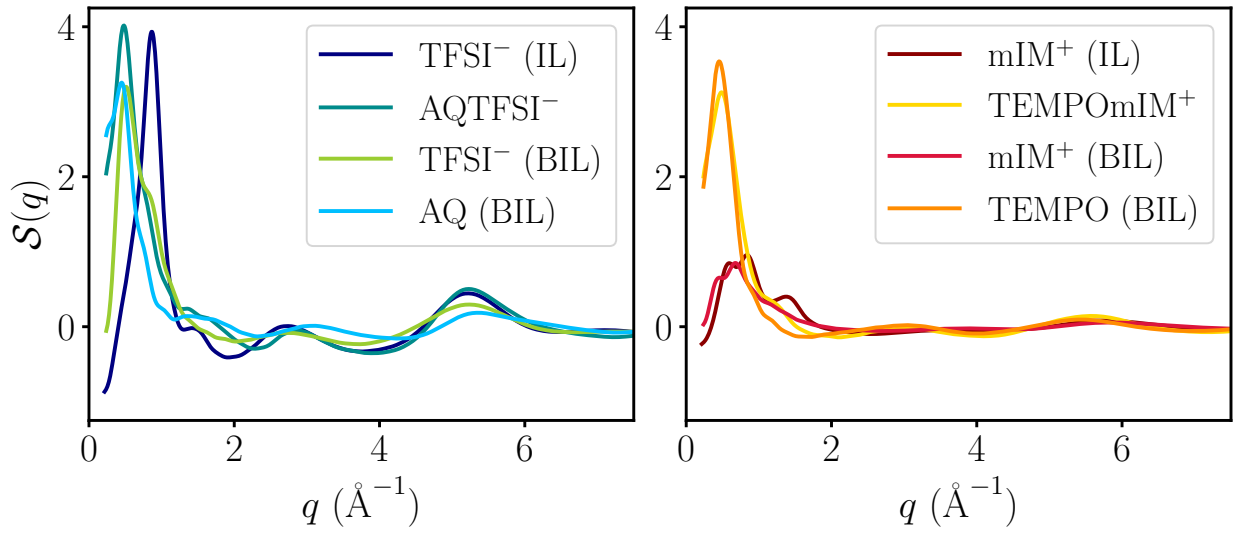

Figure 5: Partial structure factors, $S(q)$, of the AQTFSI$^-$, AQ and TFSI$^-$ groups (left) and of the TEMPOmIM$^+$, TEMPO and mIM$^+$ groups (right). For TFSI$^-$ and mIM$^+$ groups the case of the BMIM-TFSI ionic liquid is shown for comparison.

The presence of nanostructures generally has a signature on the structure factors of a liquid.[31–33] The total structure factor includes contributions that may cancel each other significantly, but it is possible to calculate specific contributions.[34–36] Here again, we have computed the partial structure factors corresponding to the four different moieties. They are compared to the ones obtained for TFSI$^-$ anions and mIM$^+$ groups in the pure 1-butyl-3-methylimidazolium (BMIM)-TFSI IL on Figure 5. In the case of the anion, we observe a very well-defined peak at 0.48 Å^{-1} for AQTFSI, which corresponds to a much longer range (of the order of 13 Å) than for TFSI$^-$ anions in the parent IL. Both the AQ and TFSI$^-$ moieties contribute to this peak since their partial structure factor almost coincides. The observation is different for cations. Although the medium-range ordering also leads to a peak at 0.49 Å^{-1}, in that case it is clearly driven by TEMPO interactions since the partial structure factor obtained for mIM$^+$ is very similar for the IL and the BIL, and much shorter-ranged. Overall, we observe a more pronounced nanostructuration of the BIL compared to the IL which can be attributed to the specific interactions evidenced before, the stacking of AQ moieties playing the main role by forming percolating domains.

In conclusion, with the aid of classical molecular dynamics, we have shown that the BIL based on anthraquinone and TEMPO functional redox groups displays strong nanostructural features, even compared to conventional ionic liquids. This is due to the peculiar affinity of the redox groups, characterized by dipole-dipole interactions between the nitroxyl functions of the TEMPO and by the stacking of the anthraquinone planes. In particular, the latter leads to the formation of large percolating domains. These structural features are likely to play a role in the good performances of BIL-based supercapacitors. The large concentration of ions allows the redox group to be in close vicinity to the electrode, and the observed nanodomains can lead to a percolation of the additional electrons or holes, a mechanism that has recently been suggested for anthraquinone-containing polymer cathodes[37] and other redox-active polymers[38] used in Li-ion batteries.

Future work should therefore focus on the understanding of the formation of the double-layer in BILs, in particular in the case of porous carbon electrodes that can induce additional nanostructuration of the liquid. Understanding completely the charging storage mechanism in BILs-based supercapacitors would in addition need to account for the redox reactions within the simulations, which requires complex methodological developments. In particular, the simulations should be able to reproduce in an effective way the electron transfers occurring at the carbon electrode interface.

Computational methods

Classical MD simulations of the BIL and of the BMIM-TFSI IL were performed using the MetalWalls software.[39,40] All the details about the polarizable force field used are described in the Supporting Information. Although this work focuses on structural properties, which are usually well reproduced by non-polarizable force fields, the dynamics of BILs is very slow and accounting for polarization is necessary to sample correctly the systems. For the BIL electrolyte, a cubic cell containing 200 BIL ion pairs was built using the PACKMOL

package.[41] A first NPT run was performed at ambient pressure for 1 ns, resulting in a cubic box with dimension $L = 54.95$ Å. The system was then annealed by increasing the temperature to 773 K in the NVT ensemble for 2 ns, and then slowly decreasing it using a ramp of 25 K every 100 ps, until the system reached a final temperature of 373 K. Then, the simulation was carried out in the NVT ensemble (at a fixed temperature of 373 K) for a total of 12 ns (2 ns of equilibration followed by 10 ns of production). For the IL, the cubic cell contained 500 IL ion pairs and was built in the same way as for the BIL electrolyte. The simulation was carried out in the NVT ensemble with a box size of 61.85 Å at a fixed temperature of 298 K, for a total of 17 ns (2 ns of equilibration followed by 15 ns of production). For the two simulations, a timestep of 1 fs was used and the trajectory was saved every 500 fs. The equations of motion were integrated using the velocity-Verlet algorithm and the temperature was kept constant using a chain Nosé-Hoover thermostat.[42,43] The short-range van der Waals interactions were calculated with a cut-off value of 12 Å, while the Ewald summation method was used for long-range and electrostatics interactions. The induced dipoles were calculated at each timestep using a conjugate-gradient procedure. Radial and dihedral distribution functions as well as structure factors and domain analysis were calculated using the TRAVIS software.[29,30] The stacking analysis was performed with an in-house written code.

Data availability

The code used for the simulations is openly available in the repository https://gitlab.com/ampere2, together with the input files for the two simulated systems.

Supporting information

Details about the polarizable force field.

Acknowledgements

This project has received funding from the European Research Council (ERC) under the European Union's Horizon 2020 research and innovation programme (grant agreement No. 771294). This work was supported by the French National Research Agency (Labex STORE-EX, Grant No. ANR-10-LABX-0076). This work was granted access to the HPC resources of CINES under Allocation A0120910463 made by GENCI.

References

1. Simon, P.; Gogotsi, Y. Perspectives for Electrochemical Capacitors and Related Devices. *Nat. Mater.* **2020**, *19*, 1151–1163.

2. Chmiola, J.; Yushin, G.; Gogotsi, Y.; Portet, C.; Simon, P.; Taberna, P. L. Anomalous Increase in Carbon Capacitance at Pore Sizes Less Than 1 Nanometer. *Science* **2006**, *313*, 1760–1763.

3. Acerce, M.; Voiry, D.; Chhowalla, M. Metallic 1T Phase MoS_2 Nanosheets as Supercapacitor Electrode Materials. *Nat. Nanotech.* **2015**, *10*, 313–318.

4. Anasori, B.; Lukatskaya, M. R.; Gogotsi, Y. 2D Metal Carbides and Nitrides (MXenes) for Energy Storage. *Nat. Rev. Mater.* **2017**, *2*, 1–17.

5. Sheberla, D.; Bachman, J. C.; Elias, J. S.; Sun, C.-J.; Shao-Horn, Y.; Dinca, M. Conductive MOF Electrodes for Stable Supercapacitors with High Areal Capacitance. *Nat. Mater.* **2017**, *16*, 220–224.

6. Salanne, M.; Rotenberg, B.; Naoi, K.; Kaneko, K.; Taberna, P.-L.; Grey, C. P.; Dunn, B.; Simon, P. Efficient Storage Mechanisms for Building Better Supercapacitors. *Nat. Energy* **2016**, *1*, 16070.

7. Balducci, A. Electrolytes for High Voltage Electrochemical Double Layer Capacitors: a Perspective Article. *J. Power Sources* **2016**, *326*, 534–540.

8. McEwen, A. B.; Ngo, H. L.; LeCompte, K.; Goldman, J. L. Electrochemical Properties of Imidazolium Salt Electrolytes for Electrochemical Capacitor Applications. *J. Electrochem. Soc.* **1999**, *146*, 1687–1695.

9. Balducci, A.; Dugas, R.; Taberna, P.-L.; Simon, P.; Plee, D.; Mastragostino, M.; Passerini, S. High Temperature Carbon-Carbon Supercapacitor Using Ionic Liquid as Electrolyte. *J. Power Sources* **2007**, *165*, 922–927.

10. Burt, R.; Breitsprecher, K.; Daffos, B.; Taberna, P.-L.; Simon, P.; Birkett, G.; Zhao, X. S.; Holm, C.; Salanne, M. Capacitance of Nanoporous Carbon-Based Supercapacitors Is a Trade-Off between the Concentration and the Separability of the Ions. *J. Phys. Chem. Lett.* **2016**, *7*, 4015–4021.

11. Mao, X.; Brown, P.; Cervinka, C.; Hazell, G.; Li, H.; Ren, Y.; Chen, D.; Atkin, R.; Eastoe, J.; Grillo, I.; Pádua, A. A. H.; Costa Gomes, M. F.; Hatton, T. A. Self-Assembled Nanostructures in Ionic Liquids Facilitate Charge Storage at Electrified Interfaces. *Nat. Mater.* **2019**, *18*, 1350–1357.

12. Mourad, E.; Coustan, L.; Lannelongue, P.; Zigah, D.; Mehdi, A.; Vioux, A.; Freunberger, S. A.; Favier, F.; Fontaine, O. Biredox Ionic Liquids with Solid-Like Redox Density in the Liquid State for High-Energy Supercapacitors. *Nat. Mater.* **2017**, *16*, 446–453.

13. Dick, L.; Stettner, T.; Liu, Y.; Liu, S.; Kirchner, B.; Balducci, A. Hygroscopic Protic Ionic Liquids as Electrolytes for Electric Double Layer Capacitors. *Ener. Storage Mater.* **2022**, *53*, 744–753.

14. Frackowiak, E.; Meller, M.; Menzel, J.; Gastol, D.; Fic, K. Redox-Active Electrolyte for Supercapacitor Application. *Faraday Discuss.* **2014**, *172*, 179–198.

15. Fic, K.; Meller, M.; Frackowiak, E. Interfacial Redox Phenomena for Enhanced Aqueous Supercapacitors. *J. Electrochem. Soc.* **2015**, *162*, A5140–A5147.

16. Evanko, B.; Yoo, S. J.; Chun, S.-E.; Wang, X.; Ji, X.; Boettcher, S. W.; Stucky, G. D. Efficient Charge Storage in Dual-Redox Electrochemical Capacitors through Reversible Counterion-Induced Solid Complexation. *J. Am. Chem. Soc.* **2016**, *138*, 9373–9376.

17. Evanko, B.; Boettcher, S. W.; Yoo, S. J.; Stucky, G. D. Redox-Enhanced Electrochemical Capacitors: Status, Opportunity, and Best Practices for Performance Evaluation. *ACS Energy Lett.* **2017**, *2*, 2581–2590.

18. Canongia Lopes, J. N. A.; Pádua, A. A. H. Nanostructural Organization in Ionic Liquids. *J. Phys. Chem. B* **2006**, *110*, 3330–3335.

19. Araque, J. C.; Hettige, J. J.; Margulis, C. J. Ionic liquids—Conventional Solvent Mixtures, Structurally Different but Dynamically Similar. *J. Chem. Phys.* **2015**, *143*, 134505.

20. Jeanmairet, G.; Rotenberg, B.; Salanne, M. Microscopic Simulations of Electrochemical Double-Layer Capacitors. *Chem. Rev.* **2022**, *122*, 10860–10898.

21. Merlet, C.; Rotenberg, B.; Madden, P. A.; Taberna, P.-L.; Simon, P.; Gogotsi, Y.; Salanne, M. On the Molecular Origin of Supercapacitance in Nanoporous Carbon Electrodes. *Nat. Mater.* **2012**, *11*, 306–310.

22. Bi, S.; Banda, H.; Chen, M.; Niu, L.; Chen, M.; Wu, T.; Wang, J.; Wang, R.; Feng, J.; Chen, T.; Dinca, M.; Kornyshev, A. A.; Feng, G. Molecular Understanding of Charge Storage and Charging Dynamics in Supercapacitors with MOF Electrodes and Ionic Liquid Electrolytes. *Nat. Mater.* **2020**, *19*, 552–558.

23. Berthin, R.; Serva, A.; Reeves, K. G.; Heid, E.; Schröder, C.; Salanne, M. Solvation of Anthraquinone and TEMPO Redox-Active Species in Acetonitrile Using a Polarizable Force Field. *J. Chem. Phys.* **2021**, *155*, 074504.

24. Mourad, E.; Coustan, L.; Freunberger, S. A.; Mehdi, A.; Vioux, A.; Favier, F.; Fontaine, O. Biredox Ionic Liquids: Electrochemical Investigation and Impact of Ion Size on Electron Transfer. *Electrochim. Acta* **2016**, *206*, 513–523.

25. Hayes, R.; Warr, G. G.; Atkin, R. Structure and Nanostructure in Ionic Liquids. *Chem. Rev.* **2015**, *115*, 6357–6426.

26. Elfgen, R.; Hollóczki, O.; Kirchner, B. A Molecular Level Understanding of Template Effects in Ionic Liquids. *Acc. Chem. Res.* **2017**, *50*, 2949–2957.

27. Tang, M.; Zhu, S.; Liu, Z.; Jiang, C.; Wu, Y.; Li, H.; Wang, B.; Wang, E.; Ma, J.; Wang, C. Tailoring Π-Conjugated Systems: From $\Pi - \Pi$ Stacking to High-Rate-Performance Organic Cathodes. *Chem* **2018**, *4*, 2600–2614.

28. Werner, D.; Apaydin, D. H.; Wielend, D.; Geistlinger, K.; Saputri, W. D.; Griesser, U. J.; Drazevic, E.; Hofer, T. S.; Portenkirchner, E. Analysis of the Ordering Effects in Anthraquinone Thin Films and Its Potential Application for Sodium Ion Batteries. *J. Phys. Chem. C* **2021**, *125*, 3745–3757.

29. Brehm, M.; Kirchner, B. TRAVIS – A Free Analyzer and Visualizer for Monte Carlo and Molecular Dynamics Trajectories. *J. Chem. Inf. Model.* **2011**, *51*, 2007–2023.

30. Brehm, M.; Thomas, M.; Gehrke, S.; Kirchner, B. TRAVIS – A Free Analyzer for Trajectories from Molecular Simulation. *J. Chem. Phys.* **2020**, *152*, 164105.

31. Urahata, S. M.; Ribeiro, M. C. C. Structure of Ionic Liquids of 1-alkyl-3-methylimidazolium Cations: A Systematic Computer Simulation Study. *J. Chem. Phys.* **2004**, *120*, 1855–1863.

32. Don Amith, W.; Hettige, J. J.; Castner, E. W.; Margulis, C. J. Structures of Ionic Liquid having both Anionic and Cationic Octyl Tails: Lamellar Vacuum Interface vs. Sponge-Like Bulk Order. *J. Phys. Chem. Lett.* **2016**, *7*, 3785–3790.

33. Borodin, O.; Suo, L.; Gobet, M.; Ren, X.; Wang, F.; Faraone, A.; Peng, J.; Olguin, M.; Schroeder, M.; Ding, M. S.; Gobrogge, E.; von Wald Cresce, A.; Munoz, S.; Dura, J. A.; Greenbaum, S.; Wang, C.; Xu, K. Liquid Structure with Nano-Heterogeneity Promotes Cationic Transport in Concentrated Electrolytes. *ACS Nano* **2017**, *11*, 10462–10471.

34. Wilson, M.; Madden, P. A. "Prepeaks" and "First Sharp Diffraction Peaks" in Computer Simulation of Strong and Fragile Ionic Liquids. *Phys. Rev. Lett.* **1994**, *72*, 3033–3036.

35. Annapuredy, H. V. R.; Kashyap, H. K.; De Biase, P.; Margulis, C. J. What is the Origin of the Prepeak in the X-ray Scattering of Imidazolium-Based Room-Temperature Ionic Liquids? *J. Phys. Chem. B* **2010**, *114*, 16838–16846.

36. Kashyap, H. K.; Hettige, J. J.; Annapuredy, H. V. R.; Margulis, C. J. SAXS Anti-Peaks Reveal the Length-Scales of Dual Positive–Negative and Polar–Apolar Ordering in Room-Temperature Ionic Liquids. *Chem. Commun.* **2012**, *48*, 5103–5105.

37. Yang, J.; Shi, Y.; Sun, P.; Xiong, P.; Xu, Y. Optimization of Molecular Structure and Electrode Architecture of Anthraquinone-Containing Polymer Cathode for High-Performance Lithium-Ion Batteries. *ACS Appl. Mater. Interfaces* **2019**, *11*, 42305–42312.

38. Wang, A.; Tan, R.; Breakwell, C.; Wei, X.; Fan, Z.; Ye, C.; Malpass-Evans, R.; Liu, T.; Zwijnenburg, M. A.; Jelfs, K. E.; McKeown, N. B.; Chen, J.; Song, Q. Solution-Processable Redox-Active Polymers of Intrinsic Microporosity for Electrochemical Energy Storage. *J. Am. Chem. Soc.* **2022**, *144*, 17198–17208.

39. Marin-Laflèche, A.; Haefele, M.; Scalfi, L.; Coretti, A.; Dufils, T.; Jeanmairet, G.; Reed, S. K.; Serva, A.; Berthin, R.; Bacon, C.; Bonella, S.; Rotenberg, B.; Madden, P. A.; Salanne, M. MetalWalls: A Classical Molecular Dynamics Software Dedicated to the Simulation of Electrochemical Systems. *J. Open Source Softw.* **2020**, *5*, 2373.

40. Coretti, A.; Bacon, C.; Berthin, R.; Serva, A.; Scalfi, L.; Chubak, I.; Goloviznina, K.; Haefele, M.; Marin-Laflèche, A.; Rotenberg, B.; Bonella, S.; Salanne, M. MetalWalls: Simulating Electrochemical Interfaces Between Polarizable Electrolytes and Metallic Electrodes. *J. Chem. Phys.* **2022**, *157*, 184801.

41. Martínez, L.; Andrade, R.; Birgin, E. G.; Martínez, J. M. PACKMOL: a Package for Building Initial Configurations for Molecular Dynamics Simulations. *J. Comput. Chem.* **2009**, *30*, 2157–2164.

42. Nosé, S. A Unified Formulation of the Constant Temperature Molecular Dynamics Methods. *J. Chem. Phys.* **1984**, *81*, 511–519.

43. Evans, D. J.; Holian, B. L. The Nose–Hoover Thermostat. *J. Chem. Phys.* **1985**, *83*, 4069–4074.